Virology 399 (2010) 322–331

Contents lists available at ScienceDirect

Virology

journal homepage: www.elsevier.com/locate/yviro

The polyomavirus BK agnoprotein co-localizes with lipid droplets

Gunhild Unterstab [a], Rainer Gosert [a], David Leuenberger [a,1], Pascal Lorentz [b], Christine H. Rinaldo [c], Hans H. Hirsch [a,d,*]

[a] Transplantation Virology, Institute for Medical Microbiology, Department of Biomedicine, University of Basel, CH-4003 Basel, Switzerland
[b] Bio-Optics Facility, Department of Biomedicine, University of Basel, Basel, Switzerland
[c] Department of Microbiology and Infection Control, University Hospital of North Norway, Tromsø, Norway
[d] Infectious Diseases and Hospital Epidemiology, University Hospital Basel, Basel, Switzerland

ARTICLE INFO

Article history:
Received 20 August 2009
Returned to author for revision
17 December 2009
Accepted 7 January 2010

Keywords:
Polyomavirus
BK virus
Agnoprotein
Accessory protein
Lipid droplets
Deconvolution
CLSM
Transfection
Infection

ABSTRACT

Agnoprotein encoded by human polyomavirus BK (BKV) is a late cytoplasmic protein of 66 amino acids (aa) of unknown function. Immunofluorescence microscopy revealed a fine granular and a vesicular distribution in donut-like structures. Using BKV(Dunlop)-infected or agnoprotein-transfected cells, we investigated agnoprotein co-localization with subcellular structures. We found that agnoprotein co-localizes with lipid droplets (LD) in primary human renal tubular epithelial cells as well as in other cells supporting BKV replication *in vitro* (UTA, Vero cells). Using agnoprotein-enhanced green fluorescent protein (EGFP) fusion constructs, we demonstrate that agnoprotein aa 20–42 are required for targeting LD, whereas aa 1–20 or aa 42–66 were not. Agnoprotein aa 22–40 are predicted to form an amphipathic helix, and mutations A25D and F39E, disrupting its hydrophobic domain, prevented LD targeting. However, changing the phosphorylation site serine-11 to alanine or aspartic acid did not alter LD co-localization. Our findings provide new clues to unravel agnoprotein function.

Introduction

Polyomaviruses (PyV) are non-enveloped double-stranded DNA viruses that have been isolated from a number of vertebrates including birds, rodents, cattle, monkeys, and humans. With few exceptions, PyV infections are little symptomatic in their natural hosts. Six PyVs have been detected in human specimens: PyV BK (BKV) and JC (JCV) in kidney, urine and brain (Chesters, Heritage, and McCance, 1983; Dorries and ter Meulen, 1983; Gardner et al., 1971; Padgett et al., 1971), KI virus and WU virus in respiratory secretions, Merkel cell carcinoma virus in a rare skin cancer, and simian virus SV40, though less consistently, in various tissues (Jiang et al., 2009). Epidemiological data in humans indicate seroprevalence rates for BKV and JCV of 82% and 58% in the general adult population (Egli et al., 2009; Knowles et al., 2003). In immunocompetent individuals, both viruses persist for life and urinary shedding is observed in 7% and 19%, respectively (Egli et al., 2009). In immunosuppressed patients, three major PyV diseases can arise: (1) PyV-associated nephropathy, caused mostly by BKV, in 1–10% of kidney transplant patients (Ramos et al., 2009). (2) PyV-associated hemorrhagic cystitis, attributed mostly to BKV, in 5–15% of allogenic hematopoietic stem cell transplant patients (Dropulic and Jones, 2008). (3) PyV-associated multifocal leukoencephalopathy caused mostly by JCV in patients with profound and persistent immunodeficiency due to hematological malignancy, advanced HIV-AIDS, or exposure to potent anti-lymphocyte agents (Jiang et al., 2009; Khanna et al., 2009). Despite the known clinical impact of BKV and JCV replication in immunosuppressed patients, effective antiviral therapy is lacking (De Clercq, 2004; Rinaldo and Hirsch, 2007). To identify potential antiviral targets of PyV replication, we are characterizing the BKV-host interaction.

Agnoprotein is one of the six major BKV proteins and expressed as a late gene, after the early genes large T- and small T-antigen at around 36 h post infection, together with the three capsid proteins VP1, VP2 and VP3 (Rinaldo et al., 1998). Although the agnoprotein is abundantly expressed *in vivo* in kidney transplant patients with nephropathy, the immune system fails to mount significant cellular and humoral responses (Leuenberger et al., 2007). BKV agnoprotein is only 66 amino acid (aa) long with an approximate 80% homology to JCV or SV40 agnoprotein suggesting a conserved function (White and Khalili, 2005). For JCV agnoprotein, diverse functions have been

* Corresponding author. Transplantation Virology, Institute for Medical Microbiology, Department of Biomedicine, University of Basel, CH-4003 Basel, Switzerland. Fax: +41 61 267 3283.
E-mail address: hans.hirsch@unibas.ch (H.H. Hirsch).
[1] Present address: Liverpool School of Tropical Medicine, Liverpool, UK.

0042-6822/$ – see front matter © 2010 Elsevier Inc. All rights reserved.
doi:10.1016/j.virol.2010.01.011

reported including negatively regulating JCV DNA replication and transcription (Safak et al., 2001), impairing the host cell response to DNA damage (Darbinyan et al., 2004), and promoting virus release by interacting with the microtubule associated protein FEZ1 (Suzuki et al., 2005). Most likely, BKV agnoprotein shares some or all of these functions, but the major function is not clear. Recent data indicated that BKV agnoprotein is phosphorylated by protein kinase C at serine-11 (Johannessen et al., 2008). Since BKV agnoprotein is highly basic (pI ≈ 10.0), it is possible that it binds to DNA as reported for SV40 agnoprotein (Jay et al., 1981). We previously observed an inhibitory effect of agnogene transfection on BKV non-coding control region-driven gene expression (Gosert et al., 2008). Given the presumably essential function in the BKV life cycle, we investigated its subcellular localization by screening cellular markers for co-localization using immunofluorescence microscopy and confocal laser scanning microscopy (CLSM). In this report we provide first evidence that agnoprotein interacts with lipid droplets via a core domain from aa 20 to 42.

Results

Subcellular distribution of agnoprotein

To analyze the subcellular distribution of agnoprotein, we infected renal proximal tubular epithelial cells (RPTECs) and Vero cells with BKV. We then performed immunofluorescence microscopy with a polyclonal antiserum directed against the agnoprotein and a monoclonal antibody directed against the viral early protein large T-antigen (LTag). BKV agnoprotein was detected in the cytoplasm while LTag was seen in the nuclei of RPTECs (Fig. 1a) and Vero cells (Figs. 1c, d). We observed that agnoprotein displayed a fine granular, almost reticular cytoplasmic distribution as well as a localization to prominent dense donut-like structures (Fig. 1b). To investigate whether or not the cytoplasmic distribution of agnoprotein was dependent on BKV infection and other viral proteins, we transiently transfected Vero cells with an agnoprotein expression vector driven by a CMV-promoter. A similar cytoplasmic distribution of agnoprotein was observed as in infected cells, with a fine reticular pattern and a prominent donut-like pattern (Figs. 1e, f). To broaden the range of immunofluorescence co-staining, we generated His- and GST-tagged agnoprotein (pCMV-agno-His, pCMV-GST-agno) and confirmed that both fusion proteins showed a distribution similar to native agnoprotein after transfection of Vero cells (data not shown). We also generated stably transfected UTA cell lines in which agnoprotein expression was under the control of a tetracycline-repressible tet-off promoter where a similar staining pattern was seen (Figs. 1g, h). The data indicate that the cytoplasmic distribution of agnoprotein to fine granular and condensed donut-like structures occurs independently of other viral proteins. Given their prominent size, we noted that the donut-like structures could be readily detected by the transmission channel of a confocal microscope (Figs. 1i–k).

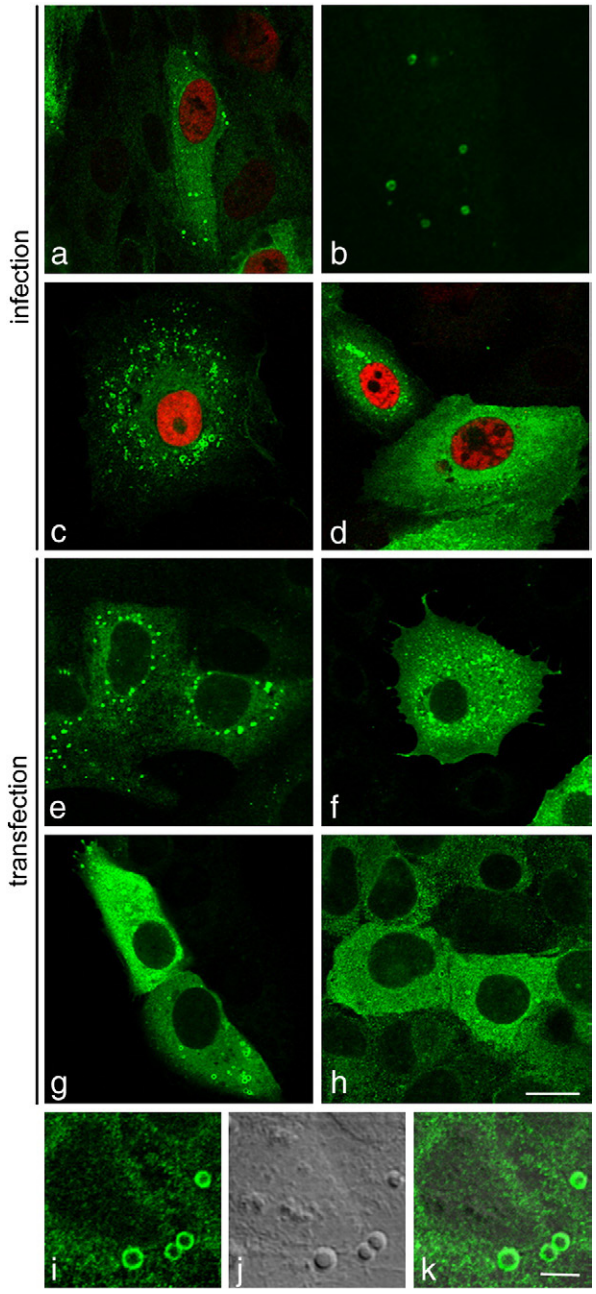

Fig. 1. The subcellular distribution of BKV agnoprotein. Confocal images of agnoprotein (green) and LTag (red) in infected RPTECs (a), with enlargement of agnoprotein specific donut-like structures (b), and Vero cells (c, d) at 72 h post infection. Detection of agnoprotein after transfection of agnoprotein gene in Vero cells (e, f) and the UTA-agno cell line (g, h). Bar 20 μm. Enlargement of agnoprotein specific donut-like structures in UTA-agno cells: (i) confocal image, (j) transmission channel and (k) merge of images shown in i and j. Bar 5 μm.

Co-localization studies of agnoprotein with cellular marker proteins

The fine granular and the donut-like patterns of agnoprotein appeared to differ in number and intensity between neighboring cells, suggesting an association with a dynamic subcellular structure. To identify the donut-like structures, we tested antibodies directed against marker proteins of various cell organelles and structures for co-localization with agnoprotein by confocal microscopy and subsequent deconvolution. Because some antibodies against cellular antigens were from rabbit, and no anti-agnoprotein antibody from mouse was available, we expressed tagged agnoprotein to allow co-staining for agnoprotein with tag-specific mouse monoclonal antibodies.

To test for association of agnoprotein with secretory structures, we first examined co-localization of tagged agnoprotein with calnexin and p63, both ER resident proteins. As judged from the staining pattern and, for p63 also from the deconvolution providing a maximum intensity projection and a corresponding three-dimensional view (isosurface), no co-localization of agnoprotein with either calnexin or p63 was apparent (Supplementary Fig. 1a, b). Next, we investigated co-localization of agnoprotein with the Golgi complex, using antibodies against beta-COP and giantin, with COPII transport vesicles, using Sar1 as a marker, and with early endosomes, by detecting the EEA1 marker protein (Supplementary Fig. 1c–f). We found no evidence for co-localization of tagged agnoprotein with any marker proteins tested. We also addressed cytosolic structures for co-localization with agnoprotein by choosing polyA-binding protein (PABP) as a marker for mRNP complexes, and the pUB-R2 protein as a

marker for the 26S proteasome but failed to detect any co-localization (Supplementary Fig. 2a, b). For JCV agnoprotein, an interaction with the heterochromatin binding protein (HP1α) has been described, which leads to an indirect interaction with the nuclear envelope (Suzuki et al., 2005). However, we could not detect co-localization with HP1α or with Lamin-A (Supplementary Fig. 2c, d).

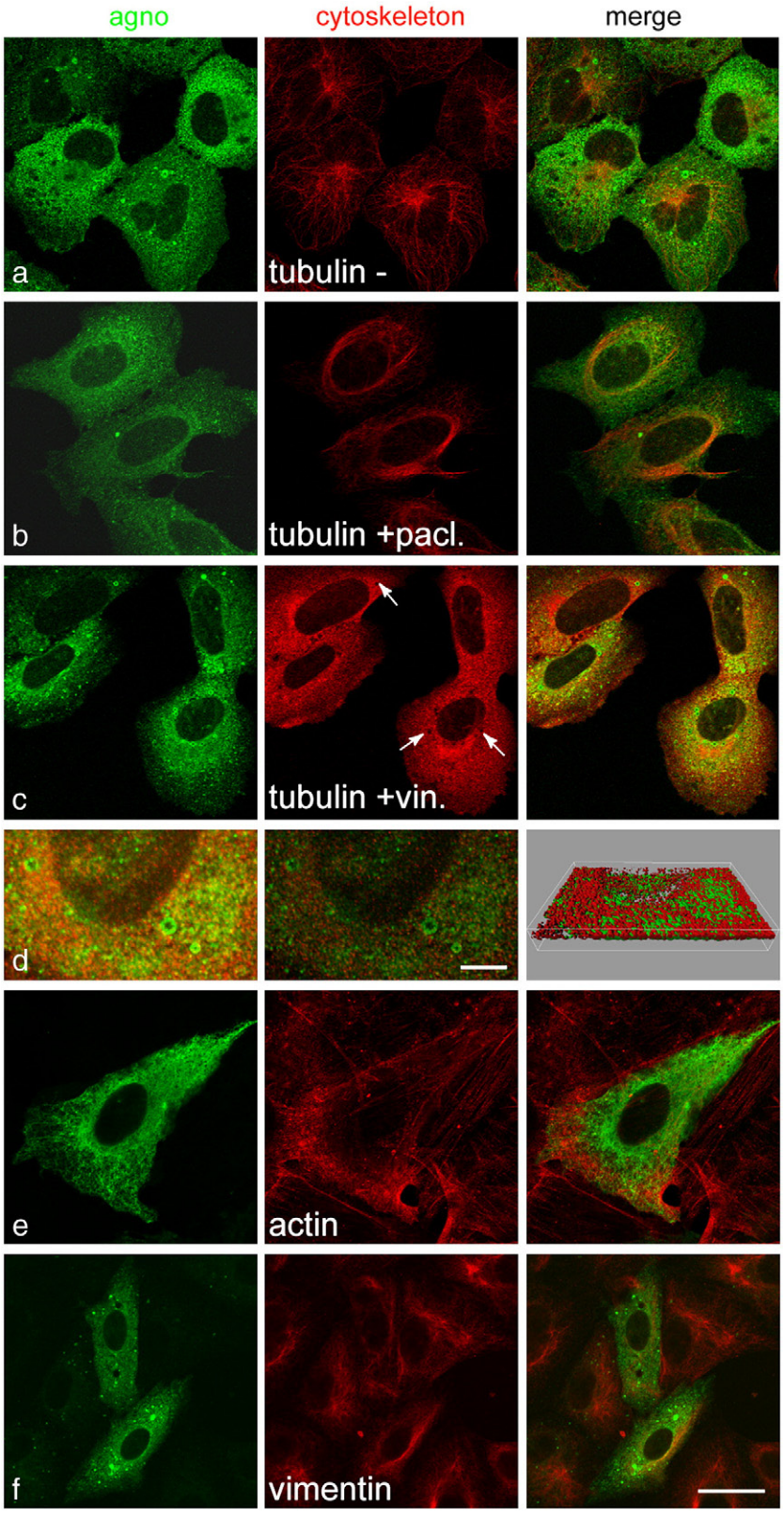

Fig. 2. Co-localization studies for BKV agnoprotein and cytoskeletal proteins. (rows a–d) Detection of agnoprotein (green) and tubulin (red) in UTA-agno-cells. (a) Cells were left untreated, (b) treated with paclitaxel, to induce microtubule stabilization or (c) treated with vincristine to depolymerize the microtubules. (d) Analysis of a z-stack from cells shown in c: Maximum-intensity projection (MIP) of a cropped stack before and after deconvolution (left and middle panel, respectively), bar 5 μm, and a corresponding three-dimensional view (isosurface). (e) Detection of agnoprotein (green) in BKV-infected RPTECs at 72 h post infection together with actin microfilaments (red). (f) Detection of agnoprotein (green) in pCMV-agno transfected Vero cells together with intermediate filament vimentin (red). Bar 20 μm.

Table 1
Target structures tested for co-localization with BKV agnoprotein using CLSM.

Target structure	Target protein	Co-Localization
ER	Calnexin	no
Rough ER	p63 (CLIMP36)	no
Endocytotic pathway	beta-COP	no
cis-Golgi	Giantin	no
Secretory pathway	Sar1	no
Endosome	EEA1	no
Translational complexes	PABP	no
Proteasome	pUB-R2	no
Nucleus	HP1α	no
Cytoskeleton	Tubulin	no
Cytoskeleton	Actin	no
Cytoskeleton	Vimentin	no
Nuclear envelope	Lamin A	no
Lysosome	LAMP1	no
P-Bodies	Hedls	no
Aggresomes	GRP78/BiP	no
Ribosomes	RPS6	no
Translational initiation	eIF3η	no
Lipid droplets	–	yes

To analyze co-localization of agnoprotein with components of the cytoskeleton, we examined microtubules, the intermediate filament vimentin, and the microfilament actin. Staining for tubulin and agnoprotein in stably transfected UTA cells indicated that agnoprotein was not co-localizing with microtubules (Fig. 2a). Treatment of UTA cells with paclitaxel, stabilizing the microtubules, did not appear to alter the distribution of agnoprotein (Fig. 2b). Treatment of cells with vincristine depolymerized microtubules and lead to homogeneously distributed tubulin dimers throughout the cytoplasm (Fig. 2c). In such cells, the fine granular distributed agnoprotein seemed to partially co-localize with the tubulin signals as evidenced by the yellow signals (Fig. 2d, left panel), but deconvolution studies indicated that this was not due to shared surfaces but due to an overlap of the green and red staining located at different levels of the stack (Fig. 2d, middle and right panel). Interestingly, the areas of agnoprotein-donuts appeared retained, spared from the tubulin signals (see arrows Fig. 2c, middle panel). Finally, we investigated the potential interaction of agnoprotein with microfilaments and intermediate filaments, using antibodies against actin and vimentin, respectively, but obtained no evidence for co-localization (Figs. 2e, f). We further extended our studies to several other inducible cellular target structures, namely P-Bodies, aggresomes, ribosomes and lysosomes. None of these structures were found to co-localize with agnoprotein (data not shown). Table 1 summarizes all marker proteins tested.

BKV agnoprotein co-localizes with lipid droplets

In order to test co-localization of agnoprotein with lipid droplets, we stained BKV-infected or agnoprotein transfected cells with LipidTOX™ and simultaneously detected agnoprotein. A significant co-localization of lipid droplets and agnoprotein became apparent. Although all cells are *per se* able to form lipid droplets, the number of lipid droplets varied in cell culture from scarce to numerous (see also Fig. 1). We therefore induced lipid droplet formation by exposing cells to oleate (Brasaemle and Wolins, 2006) (Fig. 3). A substantially higher number of agnoprotein-stained donut-like structures was seen together with an increasing number of lipid droplets compared to oleate-unexposed cells. Of note, agnoprotein-specific signals showed the characteristic donut-like appearance, whereas lipid droplets appeared like small filled vesicles. The overlay demonstrates that agnoprotein envelops each lipid droplet in agnoprotein-expressing infected or transfected cells, resulting in the typical donut-like appearance. To independently confirm our results in the absence of antibody staining, we transfected cells with an expression construct encoding an agnoprotein fused in frame to the N-terminus of enhanced green-fluorescent protein (EGFP). Following lipid droplet induction with oleate and staining with LipidTOX™, we obtained serial z-slices, resulting in a 3D image, a so called z-stack. Subsequent deconvolution was done using the Huygens professional software. This method is used to eliminate blurring and noise in order to recover the original object. Thereafter, restored images were visualized with Imaris (see Materials and methods). Two different regions of a cropped stack from a typical cell are shown (Figs. 4a–d and e–h). Fig. 4a depicts an optical slice of the deconvoluted volume. A yellow signal is visible around the lipid droplets as the result of co-localization of agnoprotein with the surface of lipid droplets. This signal became more pronounced after defining a third channel displaying areas of

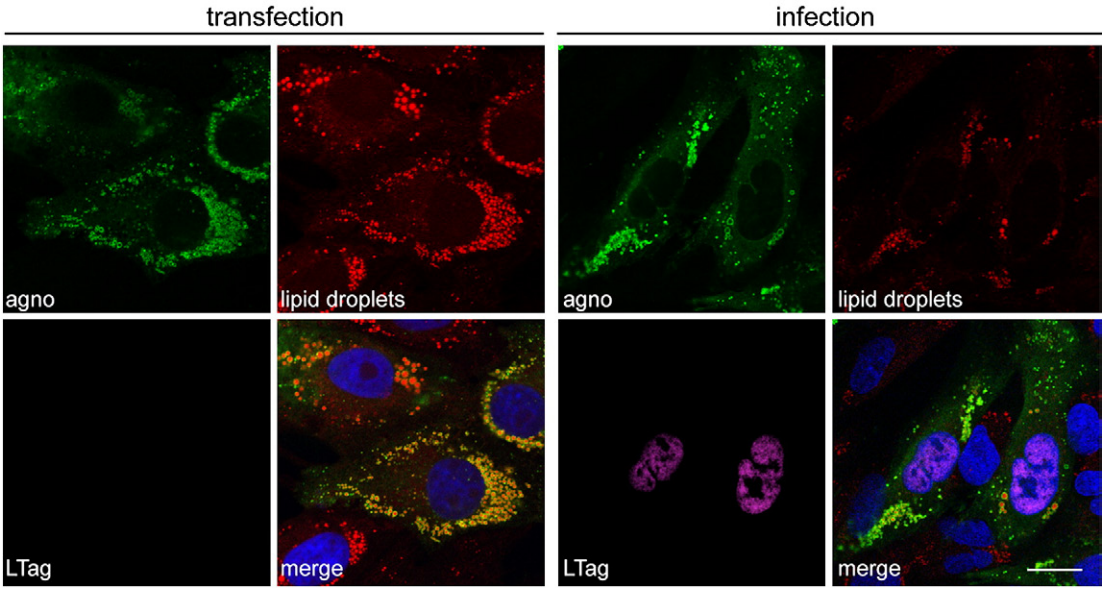

Fig. 3. BKV agnoprotein co-localizes with lipid droplets. To load cells with lipid droplets, cells were incubated with 300 μM oleate, bound to defatted BSA for 16 h. Left set: Confocal image of Vero cells, transfected with pCMV-agno prior to oleate treatment. Cells were stained for agnoprotein (green) and lipid droplets using LipidTox™ (red). Because cells were transfected and not infected, no LTag specific signal was obtained. Right set: Confocal image of BKV-infected RPTECs. Cells were treated with oleate at 24 h post infection. At 72 h post infection, the early viral protein LTag (magenta) was detected together with agnoprotein (green) and lipid droplets (red). The lower right panel of each set represents a merged image of each channel together with Hoechst stained nuclei (blue). Bar 20 μm.

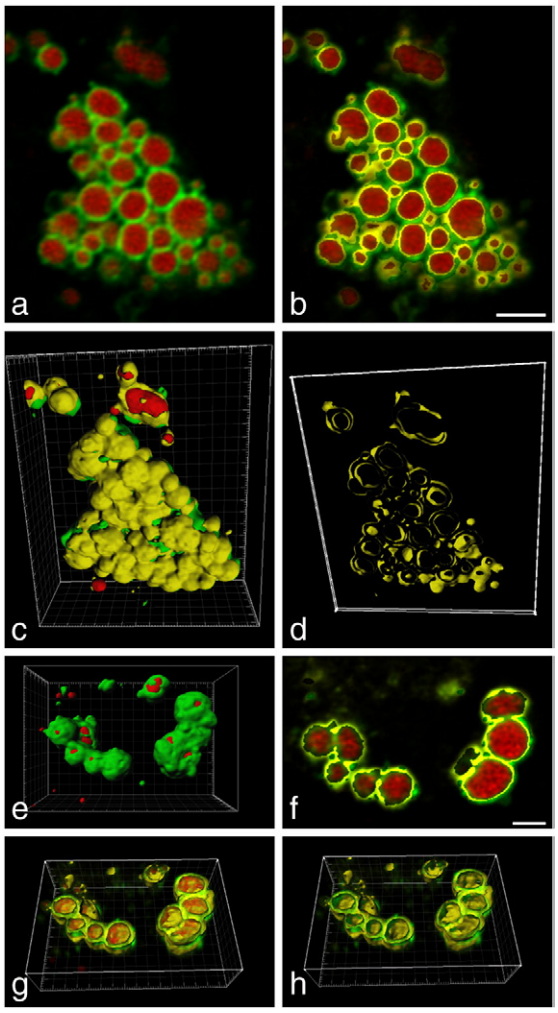

Fig. 4. BKV agnoprotein co-localizes with lipid droplets as verified by deconvolution and visualization of 3D images. Vero cells were transfected with pAgno-EGFP and loaded with lipid droplets after transfection. Cells were stained for lipid droplets and a stack of 81 slices was acquired along the z-axis. Agno-EGFP signals are shown in green and the lipid droplets are shown in red. Two different regions of a cropped stack are visualized (a–d, bar 3 μm and e–h, bar 2 μm). (a) z-slice of the deconvolved volume. (b) z-slice of the deconvolved volume with co-localizing pixels selected (Pearson coefficient 0.9305) and shown in a new channel (yellow). (c) Isosurface rendering with automatic threshold settings. (d) Visualization of a slice with manual defined thickness from the isosurface rendering, omitting the red and green channel. (e) Isosurface rendering with automatic threshold settings, omitting the co-localization channel. (f) z-slice of a deconvolved stack with co-localizing pixels selected (Pearson coefficient 0.8966) shown in a new channel (yellow). (g) Volume rendering of the deconvolved stack that was cut to allow a view inside the lipid droplet showing three channels or only the red and yellow channel (h).

co-localization in yellow, resulting in Pearson's coefficients of 0.9305 and 0.8966, respectively (Figs. 4b and f). Figs. 4c and e provide a three-dimensional view (isosurface) of the corresponding areas shown in Figs. 4a and f, demonstrating that agnoprotein almost entirely envelops the lipid droplet surface. Fig. 4d demonstrates the donut-like structure of agnoprotein distributed around lipid droplets by depicting a section of the co-localization channel. Figs. 4g and h show a cut along one plane of the isosurface model of Fig. 4e, allowing a view inside the lipid droplet. It is evident that agnoprotein interacts with the lipid droplet surface, resulting in its donut-like appearance.

The agnoprotein core of aa 20–42 mediates lipid droplet interaction

Secondary structure analysis of agnoprotein predicts aa 22–40 to form an alpha helix with amphipathic character. The hydrophobic face is composed of seven amino acids, shown in yellow, and the charged amino acids at the opposite side, shown in pink and blue (Fig. 5a). To identify the domain involved in lipid droplet targeting we constructed a set of N- and C-terminal truncated agnoprotein mutants fused to EGFP (Fig. 5a). We transfected Vero cells with the different expression constructs and verified the expression of the indicated fusion proteins by Western blot (Fig. 5a). Co-localization with lipid droplets was studied with or without lipid droplet induction (Fig. 5b). As shown, agno(1-42)- and agno(20-66)-EGFP fusion proteins, both containing the predicted helix co-localized with lipid droplets as observed for the full-length agno-EGFP. In contrast, agno(1-20)- and agno(42-66)-EGFP, both lacking the predicted helix failed to target lipid droplets. We therefore concluded that aa 20–42 are necessary for directing agnoprotein to lipid droplets. To further validate our hypothesis, we disrupted the amphipathic character of the helix by specific point mutations previously described for RNaseE in *Escherichia coli* (Khemici et al., 2008). Accordingly, we generated a full-length agnoprotein mutant in which alanine at position 25 was replaced with aspartic acid (25D) and phenylalanine at position 39 with glutamic acid (39E). As shown, agno(25D39E)-EGFP did not target lipid droplets (Fig. 5c) but instead displayed a cellular distribution in cytoplasm and nucleus indistinguishable from EGFP alone (Fig. 5b). To independently investigate the distribution of mutant 25D39E agnoprotein, we used the agno specific antiserum for IF and confirmed co-localization with the EGFP signal in the cytoplasm and in the nucleus (Fig. 5c, lower row). From these data, we concluded that the agnoprotein core of aa 20–42 is not only necessary to mediate co-localization with lipid droplets, which required the hydrophobic domain of the amphipathic helix, but also to mediate the preferential retention in the cytoplasm. As phosphorylation of agnoprotein at serine-11 by PKC has been suggested to modulate its effect on virus replication (Johannessen et al., 2008), we constructed an agno-EGFP fusion protein replacing serine at position 11 with aspartic acid (11D). We found that the mutant agno(11D)-EGFP targeted lipid droplets (Fig. 5d). Similarly, changing serine-11 into alanine, which prevents phosphorylation at this site, also did not alter co-localization with lipid droplets (data not shown).

Discussion

In this study, we conducted a detailed analysis of the subcellular distribution of the BKV agnoprotein using immunofluorescence microscopy and CLSM. We observed that agnoprotein is distributed in two patterns in the cytoplasm, one being fine granular, the other being large and donut-like. Screening several cellular markers for co-localization, we were able to exclude association with a number of cellular structures (Table 1). However, we found that agnoprotein co-localizes with lipid droplets presenting as donut-like structures. This

Fig. 5. BKV agnoprotein secondary structure prediction and EGFP-fusion constructs. (a) Secondary structure prediction of the BKV agnoprotein was performed on the NPSA website using the HNN tool (http://pbil.ibcp.fr/htm/index.php). The server predicts formation of a helix within aa 22–40. Illustration of the predicted amphipathic structure as a helical wheel, drawn using the Helical Wheel Viewer on the website http://cti.itc.virginia.edu/~cmg/Demo/wheel/wheelApp.html. aa 22–39 are shown (highlighted in yellow); nonpolar aa (orange), polar, uncharged aa (green), acidic aa (pink), and basic aa (blue). Schematic presentation of agnoprotein-EGFP fusion constructs indicating the aa in parenthesis and deleted parts as dotted line. The helix from aa 22–40 is shown as a blue barrel. Expression of the fusion proteins was verified by Western blot using an anti-GFP antibody. (b, c, d) Confocal images of Vero cells transfected with EGFP and different pAgno-EGFP fusion constructs as indicated in (a) either without (−) or after 0.3 mM oleate exposure for 16 hours. Agno-EGFP is shown in green, lipid droplets in red (LipidTOX™) and nuclei in blue (Hoechst 33342). Regions of co-localization appear yellow in the merge panel. (c, lower row) Confocal images of Vero cells transfected with pAgno25D39E-EGFP expression construct to confirm proper expression of the agno25D39E-EGFP fusion protein. Agnoprotein was detected using an agno-specific antiserum (magenta), EGFP specific signals are shown in green. Co-localization of both signals is shown in the merge panel. Bar 20 μm.

a

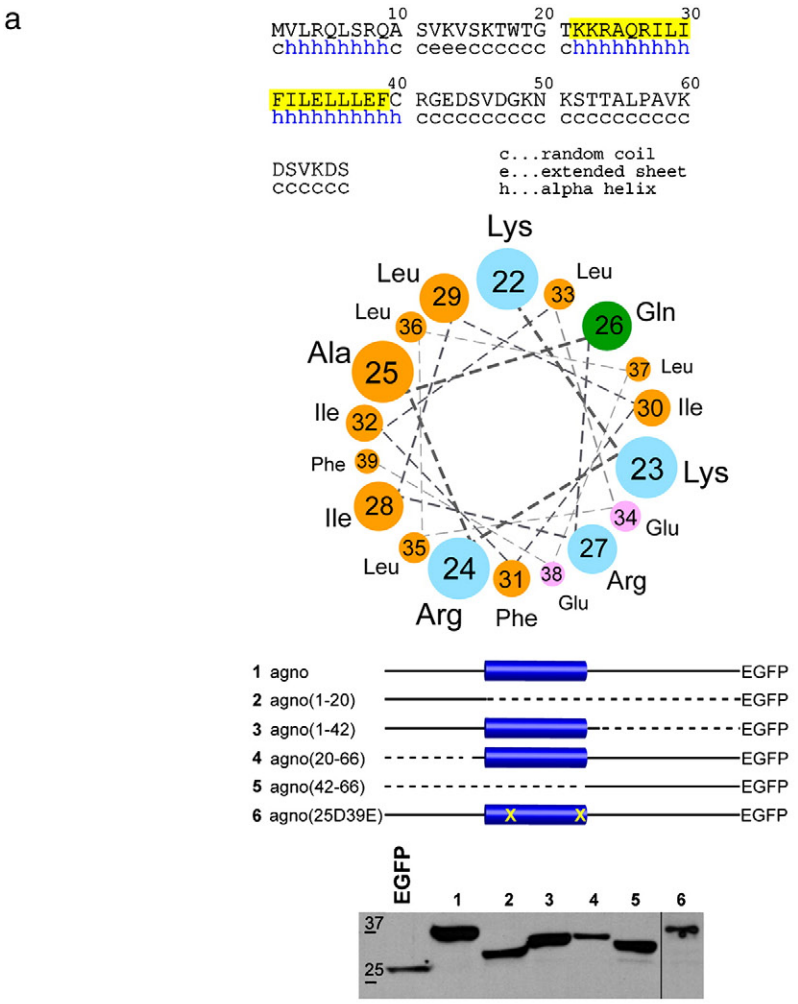
MVLRQLSRQA SVKVSKTWTG TKKRAQRILI
chhhhhhhhc ceeeccccccc chhhhhhhhh
FILELLLEFC RGEDSVDGKN KSTTALPAVK
hhhhhhhhhh ccccccccccc ccccccccccc
DSVKDS
cccccc
c...random coil
e...extended sheet
h...alpha helix
Lys 22
Leu 29
Leu 33
Leu 36
Gln 26
Ala 25
37 Leu
Ile 32
30 Ile
Phe 39
23 Lys
Ile 28
34 Glu
35 Leu
24 Arg
31 Phe
27 Arg
38 Glu
1 agno EGFP
2 agno(1-20) EGFP
3 agno(1-42) EGFP
4 agno(20-66) EGFP
5 agno(42-66) EGFP
6 agno(25D39E) EGFP
EGFP
1 2 3 4 5 6
37
25

b

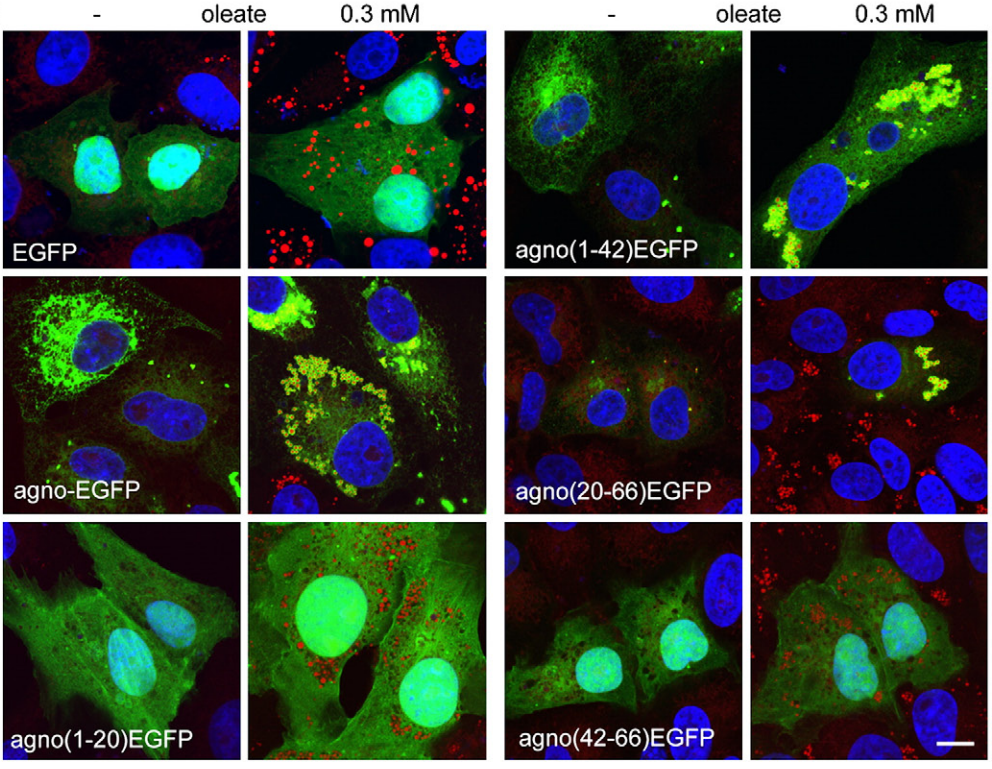
- oleate 0.3 mM
- oleate 0.3 mM
EGFP
agno(1-42)EGFP
agno-EGFP
agno(20-66)EGFP
agno(1-20)EGFP
agno(42-66)EGFP

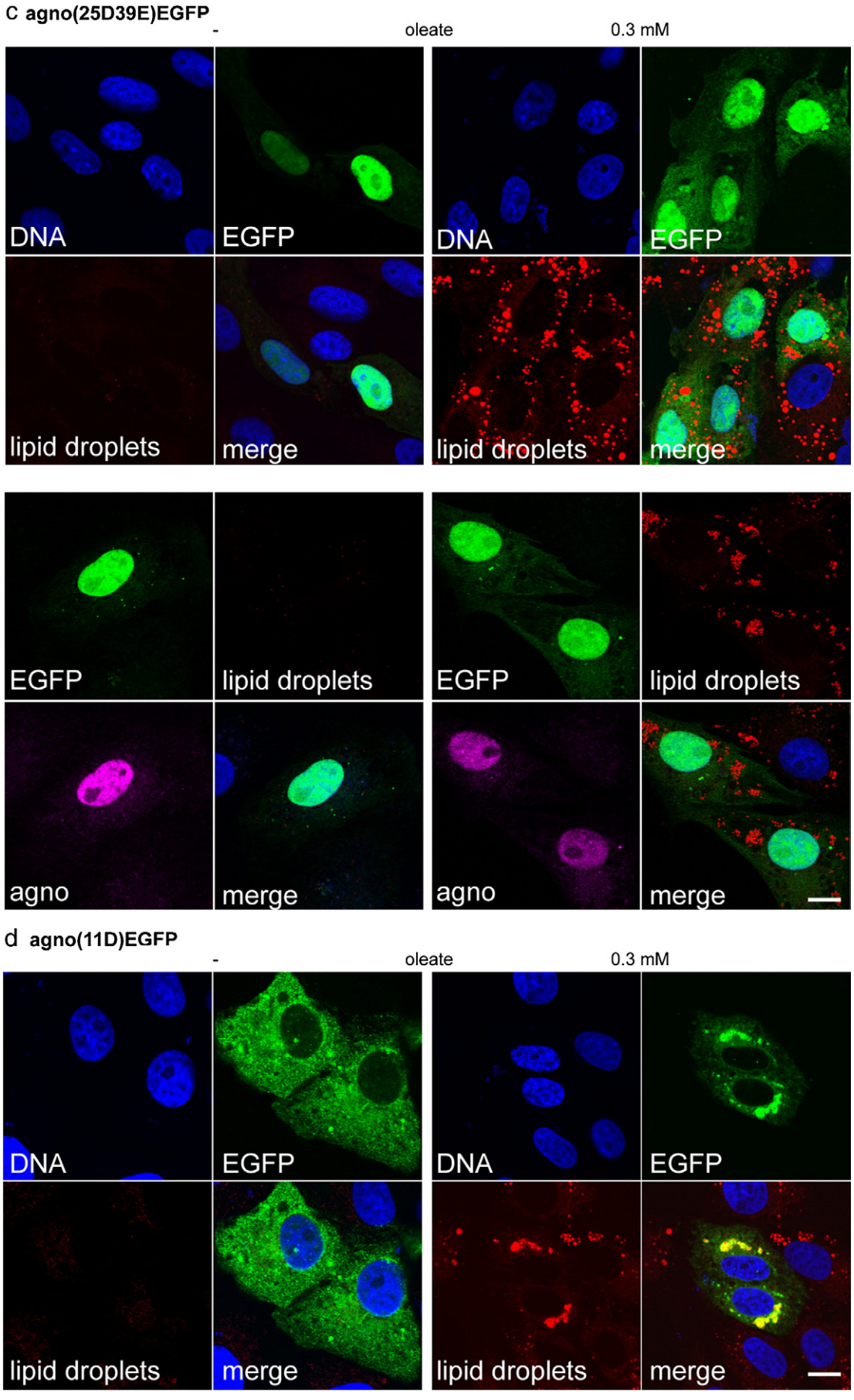

Fig. 5 (*continued*).

interaction was observed in different cell types including RPTECs, Vero and UTA cells and became significantly more prominent when lipid droplets were induced by exposure to oleate. We independently verified this interaction by using agnoprotein-EGFP fusion proteins. Moreover, by constructing N-terminal and C-terminal truncations of agnoprotein, we provide evidence that the agnoprotein core from aa 20–42 is necessary to mediate lipid droplet targeting. The secondary structure of this core region is predicted to form an amphipathic helix, a structure known to mediate associations to lipid surfaces (van Kuppeveld et al., 1997). Accordingly, two point mutations at positions 25 and 39, which disrupt the hydrophobic domain of the amphipathic helix by introducing negatively charged aa, were sufficient to prevent agnoprotein-EGFP association with lipid droplets. Conversely, mutant agno-EGFP fusion proteins lacking the helix or having a disturbed amphipathic helix were no longer exclusively retained in the cytoplasm but were also present in the nucleus of the cells in both untreated and oleate-treated cells. This observation suggests that the amphipathic helix also is a major determinant of the cytoplasmic retention of the agnoprotein. Changing phosphorylation site at serine-11 to either aspartic acid to simulate phosphorylation, or to alanine to prevent phosphorylation, did not affect lipid droplet targeting of agnoprotein.

Lipid droplets are highly dynamic organelles that consist of a hydrophobic core composed of neutral lipids, mostly triacylglycerol and sterolesters, surrounded by a polar phospholipid monolayer. Numerous proteins have been identified that attach to this membrane and their number is growing. Recent work from different groups has aimed at elucidating the lipid droplet proteome (Brasaemle et al., 2004). Most interestingly, some proteins only temporarily localize to lipid droplets and seem not primarily related to lipid metabolism (for reviews, see Welte, 2007; Zehmer et al., 2009). Some proteins detected in lipid droplets are also involved in vesicle transport, RNA splicing, transcription as well as translation (Guo et al., 2008). It is clear today, that virtually all eukaryotic cells are able to form lipid droplets, in addition to adipocytes specialized in fat metabolism. Lipid droplets appear to travel rapidly along microtubules and transiently interact with various cellular organelles including endosomes (Liu et al., 2007). Moreover, it has been proposed that lipid droplets are also communicating with peroxisomes, mitochondria, lysosomes and the ER via so called “transient inter-compartmental contact sites” (Zehmer et al., 2009).

Our observation that the BKV agnoprotein targets lipid droplets raises the question of the biological relevance of this interaction, particularly in the late phase of the polyomavirus replication cycle. At least three intracellular pathogens are taking advantage of lipid droplets. The core proteins of HCV and the closely related GB virus-B localize to lipid droplets (Barba et al., 1997; Hope et al., 2002) to recruit nonstructural proteins as well as the viral RNA replication complexes to lipid droplet-associated membranes (Miyanari et al., 2007). On the other hand, the intracellular bacterium *Chlamydia trachomatis* secretes a protein that targets lipid droplets to redirect and exploit this source of lipids (Kumar et al., 2006). We noted that association of BKV agnoprotein with lipid droplets occurs even in the presence of little agnoprotein expression. Also, this interaction is seen spontaneously, in the absence of deliberate lipid droplet induction with oleate. These observations suggest that the presence of lipid droplets in the cell is a strong dynamic determinant for the subcellular localization of agnoprotein. In fact, we observed that JCV agnoprotein also co-localizes with lipid droplets (unpublished data). Re-appreciation of the work from Shishido-Hara et al. independently supports that JCV agnoprotein distributes to fine granular as well as to donut-like structures (Shishido-Hara et al., 2004).

Protein targeting to lipid droplets has been studied for several proteins that interact with lipid droplets, including perilipin A, the HCV core protein, the closely related GBV-B core protein (Hope and McLauchlan, 2000; Hope et al., 2002; Subramanian et al., 2004) and caveolin-1 (Ostermeyer et al., 2004). From these data, no consensus sequence for targeting lipid droplets can be defined. Rather, different modes of interaction seem to exist which include amphipathic helices as predicted for the agnoprotein core aa 20–42. At present, the role of agnoprotein in the context of lipid droplets remains speculative. Cultured RPTECs, the natural target cells for BKV replication in BKV-associated nephropathy show only a few lipid droplets when maintained under tissue culture conditions. In the kidney, however, the situation might be different (Nast and Cohen, 1985). For RPTECs and other cells, it has been shown that fatty acids induce oxidative stress and apoptosis and that one way to protect cells, is the esterification to form triacylglycerol and cholesterol esters that are stored in lipid droplets (Ishola et al., 2006; Urahama et al., 2008). Thus, it is possible that lipid droplets might be disadvantageous for viral replication, which is counteracted by agnoprotein. Also, agnoprotein might facilitate lipid droplet degradation or promote viral egress (Myhre et al., 2010). Recent work observed that pravastatin, a cholesterol-lowering agent represses BKV replication (Moriyama and Sorokin, 2008). Our observation that the BKV agnoprotein co-localizes to lipid droplets is surprising and will provide new insights not only into its role in the viral life cycle but may prove to be another example of how small DNA viruses may be useful probes for the study of as yet incompletely defined cellular functions.

Materials and methods

Cell culture and reagents

Vero cells (ATCC CRL1587) were grown in DMEM (6046, Sigma, St. Louis, MO), supplemented with 10% fetal bovine serum and 2 mM L-glutamine (S0113 and K0302, respectively, Biochrome AG, Berlin, Germany). Human renal proximal tubular epithelial cells (RPTECs) (Sc-4100) were purchased from ScienCell Laboratories, San Diego, and maintained in epithelial cell medium (EpiCM, Sc-4101). For passaging of cells, passage kit 2 (2040002) was used. The UTA-agno-11 cell line, which expresses the BKV agnoprotein in a tetracycline-dependent manner, was derived from the osteosarcoma cell line U2OS. Briefly, U2OS cells were stably transfected with the regulatory plasmid encoding for the transactivator and selected with G418 to yield clone UTA 6 (Englert et al., 1995). These cells were then transfected with the agnoprotein-encoding construct pTRE-agno that confers puromycin resistance. Puromycin-resistant clones were selected to yield the cell line UTA-agno-11. This cell line was maintained in DMEM (6046, Sigma), supplemented with 10% fetal bovine serum and 2 mM L-glutamine (S0113 and K0302, respectively, Biochrome AG), 500 μg/ml G418, 1.5 μg/ml puromycin, and 1 μg/ml tetracycline. To induce agnoprotein expression, cells were cultivated in the absence of tetracycline for 48 h. For manipulation of the microtubule network, cells were treated with 1 μM vincristine (V8388) or paclitaxel (T7402) (Sigma) for 4 h. To induce lipid droplets, culture medium was supplemented with 300 μM oleate (O1383, Sigma) bound to essentially fatty acid free bovine albumin (A6003, Sigma) as described (Brasaemle and Wolins, 2006).

Expression plasmids and reagents

The pCMV-agno (pRC-agno) and pTRE-agno constructs have been described (Leuenberger et al., 2007; Rinaldo et al., 1998). pCMV-GST-agno, encoding for agnoprotein fused to the C-terminus of GST, was generated by subcloning the GST-BKVagno fragment (*BspEI–NotI*) from pFastBacGST-BKVagno (Leuenberger et al., 2007) into *XmaI–NotI* cut pEGFP-N1 replacing the EGFP-N1 coding sequence. To construct the pcDNA-agno-HIS expression plasmid, encoding for a C-terminal HIS tagged agnoprotein, the agno-encoding sequence was amplified using the forward primer 5'-GGTTGGGCTAGCATGGTTCTGCGCCAG-3′

and the reverse primer 5'-TTTTTTCTCGAGTCAATGATGATGATGATGATGACCGGAGTCTTTTACAGAGTCT-3′ with pCMV-agno as template. The *NheI–XhoI* insert was ligated into the pcDNA3.1 plasmid. To obtain an expression plasmid for an agno-EGFP fusion protein, with EGFP fused on the C-terminus of the agnoprotein, the agno-encoding sequence was amplified using the forward primer 5'-GCGAATTCACCATGGTTCTGCGC-3′ and reverse primer 5'-GCGGATCCCGCAAGGAGTCTTTTAC-3′, thereby introducing *EcoRI* and *BamHI* restriction sites and eliminating the stop codon of the agno-coding sequence. For C-terminal truncation mutants agno 1–20 and agno 1–42, the reverse primers 5'-GCGGATCCCGTCCAGTCCAGGTTTTACC-3′ and 5'-GCGGATCCCGACCTCTACAAAATTCCAGC-3′ were used, respectively, together with the forward primer described for full-length agno-EGFP.

For the N-terminal truncation mutants agno20-66 and agno42-66, we used the forward primers 5'-GCGAATTCACCATGGGAACAAAAAAAAGAGC-3' and 5'-GCGAATTCACCATGGGTGAAGACAGTGTAGACG-3' together with the reverse primer described for full-length agno-EGFP.

The *EcoRI–BamHI* digested PCR product was ligated into accordingly digested pEGFP-N1, resulting in pAgno-EGFP. The point mutation agnoproteins A25D F39E, and S11D were obtained by synthesizing the *EcoRI–BamHI* insert (Eurogentec, Liège, Belgium) and ligating it into pEGFP-N1 as described above. Aa exchange of Ala→Asp at position 25 was introduced by changing the codon GCT into GAT and aa exchange of Phe→Glu at position 39 by changing the codon TTT into GAA. Ser→Asp exchange at position 11 was introduced by changing the codon TCT into GAT. All constructs were verified by sequencing.

Transfection and infection

Transfection was done using Lipofectamine2000 (Invitrogen, Carlsbad, CA) according to manufacturers instructions. RPTEC and Vero cells were infected with BKV (Dunlop) containing Vero cell supernatants as described previously for human umbilical vein epithelial cells (Grinde et al., 2007).

Immunofluorescence (IF) and antibodies

Cells were fixed with 4% paraformaldehyde at room temperature for 10 min and permeabilized with 0.2% Triton at room temperature for 10 min. For the use of the anti-actin antibody cells were permeabilized with ice-cold methanol at room temperature for 5 min. For the detection of lipid droplets, permeabilization was done with 0.05% Saponin (S7900, Sigma) in PBS. All solutions used thereafter contained 0.05% Saponin. After incubation with primary antibodies, diluted in 3% BSA/PBS, at room temperature for 1 h, cells were washed three times with PBS and incubated with secondary fluorescently labeled antibodies, diluted in 3% BSA/PBS, at room temperature for 45 min. After three washes, IF specimens were mounted in 90% Glycerol (1.04095, Merck, Darmstadt, Germany) in PBS, containing 1% *N*-propyl gallate (P-3130, Sigma) as antifading agent.

Primary antibodies were used as followed: anti-agnoprotein antiserum 1:800 (Rinaldo et al., 1998); anti-p63 (G1/296) 1:1000, anti-Giantin (G1/133) 1:400, anti-LAMP1 (G1/139) 1:1000 were kind gifts from HP Hauri (Biozentrum, University of Basel) (Linstedt and Hauri, 1993; Schweizer et al., 1993; Schweizer et al., 1988); anti-Sar1 1:500 kind gift from FT Wieland (Biochemistry Center, Heidelberg University), anti-beta-COP 1:30 kind gift from BL Tang (University of Singapore) (Rust et al., 2001). Commercially available antibodies were used as followed: anti-actin 1:200 (ab40864, Abcam, Cambridge, MA), anti-calnexin 1:200 (SPA-860, StressGen, San Diego, CA), anti-EEA1 1:100 (610456, BD Biosciences, San Jose, CA), anti-His 1:300 (DIA900, Dianova, Hamburg, Germany), anti-HP1α 1:50 (05-689, Upstate Biotechnology, Billerica, MA), anti-LaminA 1:200 (ab8980, Abcam), anti-PABP 1:50 (P6246, Sigma), anti-tubulin 1:200 (A-11126, Molecular Probes, Carlsbad, CA), anti-vimentin 1:40 (V6389, Sigma); anti-eIFη 1:200 (sc-16378), anti-GRP78 1:100 (sc-1051), anti-pUB-R2 1:25 (sc-13725), anti-p70s6k 1:500 (sc-8416) and anti-RPS6 1:25 (sc-13007) were all from Santa Cruz Biotechnology (Santa Cruz, CA). Anti-SV40Tag 1:50 (DP02, Calbiochem, San Diego, CA) cross-reacts with BKV-LTag. Lipid droplets were visualized using LipidTOX™ (34476, Invitrogen) at a 1:1000 dilution in the secondary antibody mixture.

Secondary antibodies were chosen depending on the primary antibodies used: for triple staining, the following combinations were used: LipidTOX™, anti-mouse-Alexa 647 1:200 (A-21463, Molecular Probes), anti-rabbit-Alexa 488 1:1000 (A-21441, Molecular Probes) or LipidTOX™, EGFP, anti-rabbit-Alexa 633 1:400 (A-21071, Molecular Probes). For double labeling, anti-mouse-Alexa 488 1:800 (A-11029, Molecular Probes) and anti-rabbit-Cy3 1:2000 (111-165-144, Jackson Immunoresearch, West Grove, PA) or anti-goat-Cy3 1:600 (705-165-003, Jackson Immunoresearch) and anti-rabbit-Alexa 488 were combined. DNA was stained by Hoechst 33342 dye (0.5 μg/ml, H21492, Invitrogen). In order to show agno-specific signals consistently in green, channels were switched if necessary.

Confocal laser scanning microscopy (CLSM)

Digital optical sections were taken with a confocal laser scanning microscope (Zeiss LSM 510 Meta, Carl Zeiss AG, Oberkochen, Germany), using a 40 Plan-Neofluar/NA1.3 oil or a 63 Plan-Apochromat/NA1.4 oil objective. Depending on the different fluorochrome-tagged secondary antibodies following lasers were used: Enterprise 405 nm; laser line 488 nm of the Argon laser, He–Ne 514 nm, He–Ne 633 nm. To exclude the possibility of channel crosstalk, images were acquired sequentially using the multi-track mode.

For z-stacks acquisition of EGFP and LipidTox™ fluorescent specimen, the requirements of the Nyquist theorem were fulfilled, with voxel xyz size of 50, 50, 160 nm, respectively. The stack contained 81 optical slices. Deconvolution and visualization was done essentially as described (Rust et al., 2001). For deconvolution, the Huygens professional software (Scientific Volume Imaging, Hilversum, the Netherlands) was used, applying the Classic Maximum Likelihood Estimation Mode (CMLE) using a theoretical point spread function (PSF). The signal to noise ratio was set at 15 and 20 for green (channel 1) and red (channel 2), respectively, and the background was set to a value of 100. For 3D-rendering and data analysis, the Imaris software (Bitplane AG, Zürich, Switzerland) was used. Co-localizing pixels were visualized by defining a third channel (yellow), resulting in Pearson's coefficients of 0.9305 and 0.8966 for pictures 6a–d and 6e–h, respectively.

Western blot

Western blot was performed as described (Gosert et al., 2008). Briefly, transfected cells were lysed in RIPA buffer (150 mM NaCl, 50 mM Tris–HCl, pH 8.0, 1% NP-40, 0.5% deoxycholate, 0.1% SDS, and protease inhibitors [Roche]) at 24 h post transfection. Cell lysates were separated by SDS-PAGE and electrotransferred onto 0.2 μm nitrocellulose membrane (Whatman). The primary anti-GFP (ab1218, Abcam) was diluted 1:1000. Secondary anti-mouse HRP conjugated antibody (P0447, DAKO, Glostrup, Denmark) was used at a 1:3000 dilution. For detection the SuperSignal West Dura Kit was used (Thermo Fisher Scientific, Rockford, IL).

Acknowledgments

We thank F.T. Wieland for the anti-Sar1 antiserum, B.L. Tang for providing us with the anti-beta-COP antibody, and H.P. Hauri for the antibodies against p63, giantin and LAMP1. We are grateful to J. Hagmann for help with deconvolution and M. Wernli for excellent technical assistance. This study was supported in part by Swiss National Fonds Grant 3200B0-110040/1 to H.H.H.

Appendix A. Supplementary data

Supplementary data associated with this article can be found, in the online version, at doi:10.1016/j.virol.2010.01.011.

References

Barba, G., Harper, F., Harada, T., Kohara, M., Goulinet, S., Matsuura, Y., Eder, G., Schaff, Z., Chapman, M.J., Miyamura, T., Brechot, C., 1997. Hepatitis C virus core protein shows a cytoplasmic localization and associates to cellular lipid storage droplets. Proc. Natl. Acad. Sci. U.S.A. 94 (4), 1200–1205.

Brasaemle, D.L., Wolins, N.E., 2006. Isolation of lipid droplets from cells by density gradient centrifugation. Curr. Protoc. Cell Biol. Chapter 3, Unit 3 15.

Brasaemle, D.L., Dolios, G., Shapiro, L., Wang, R., 2004. Proteomic analysis of proteins associated with lipid droplets of basal and lipolytically stimulated 3T3-L1 adipocytes. J. Biol. Chem. 279 (45), 46835–46842.

Chesters, P.M., Heritage, J., McCance, D.J., 1983. Persistence of DNA sequences of BK virus and JC virus in normal human tissues and in diseased tissues. J. Infect. Dis. 147 (4), 676–684.

Darbinyan, A., Siddiqui, K.M., Slonina, D., Darbinian, N., Amini, S., White, M.K., Khalili, K., 2004. Role of JC virus agnoprotein in DNA repair. J. Virol. 78 (16), 8593–8600.

De Clercq, E., 2004. Antivirals and antiviral strategies. Nat. Rev. Microbiol. 2 (9), 704–720.

Dorries, K., ter Meulen, V., 1983. Progressive multifocal leucoencephalopathy: detection of papovavirus JC in kidney tissue. J. Med. Virol. 11 (4), 307–317.

Dropulic, L.K., Jones, R.J., 2008. Polyomavirus BK infection in blood and marrow transplant recipients. Bone Marrow Transplant. 41 (1), 11–18.

Egli, A., Infanti, L., Dumoulin, A., Buser, A., Samaridis, J., Stebler, C., Gosert, R., Hirsch, H.H., 2009. Prevalence of Polyomavirus BK and JC Infection and Replication in 400 Healthy Blood Donors. J. Infect. Dis. 199, 837–846.

Englert, C., Hou, X., Maheswaran, S., Bennett, P., Ngwu, C., Re, G.G., Garvin, A.J., Rosner, M.R., Haber, D.A., 1995. WT1 suppresses synthesis of the epidermal growth factor receptor and induces apoptosis. EMBO J. 14 (19), 4662–4675.

Gardner, S.D., Field, A.M., Coleman, D.V., Hulme, B., 1971. New human papovavirus (B.K.) isolated from urine after renal transplantation. Lancet 1 (7712), 1253–1257.

Gosert, R., Rinaldo, C.H., Funk, G.A., Egli, A., Ramos, E., Drachenberg, C.B., Hirsch, H.H., 2008. Polyomavirus BK with rearranged noncoding control region emerge in vivo in renal transplant patients and increase viral replication and cytopathology. J. Exp. Med. 205 (4), 841–852.

Grinde, B., Gayorfar, M., Rinaldo, C.H., 2007. Impact of a polyomavirus (BKV) infection on mRNA expression in human endothelial cells. Virus Res. 123 (1), 86–94.

Guo, Y., Walther, T.C., Rao, M., Stuurman, N., Goshima, G., Terayama, K., Wong, J.S., Vale, R.D., Walter, P., Farese, R.V., 2008. Functional genomic screen reveals genes involved in lipid-droplet formation and utilization. Nature 453 (7195), 657–661.

Hope, R.G., McLauchlan, J., 2000. Sequence motifs required for lipid droplet association and protein stability are unique to the hepatitis C virus core protein. J. Gen. Virol. 81 (Pt. 8), 1913–1925.

Hope, R.G., Murphy, D.J., McLauchlan, J., 2002. The domains required to direct core proteins of hepatitis C virus and GB virus-B to lipid droplets share common features with plant oleosin proteins. J. Biol. Chem. 277 (6), 4261–4270.

Ishola Jr., D.A., Post, J.A., van Timmeren, M.M., Bakker, S.J., Goldschmeding, R., Koomans, H.A., Braam, B., Joles, J.A., 2006. Albumin-bound fatty acids induce mitochondrial oxidant stress and impair antioxidant responses in proximal tubular cells. Kidney Int. 70 (4), 724–731.

Jay, G., Nomura, S., Anderson, C.W., Khoury, G., 1981. Identification of the SV40 agnogene product: a DNA binding protein. Nature 291 (5813), 346–349.

Jiang, M., Abend, J.R., Johnson, S.F., Imperiale, M.J., 2009. The role of polyomaviruses in human disease. Virology 384 (2), 266–273.

Johannessen, M., Myhre, M.R., Dragset, M., Tummler, C., Moens, U., 2008. Phosphorylation of human polyomavirus BK agnoprotein at Ser-11 is mediated by PKC and has an important regulative function. Virology 379 (1), 97–109.

Khanna, N., Elzi, L., Mueller, N.J., Garzoni, C., Cavassini, M., Fux, C.A., Vernazza, P., Bernasconi, E., Battegay, M., Hirsch, H.H., for the Swiss HIV Cohort Study, 2009. Incidence and outcome of progressive multifocal leukoencephalopathy in 20 years of the Swiss HIV Cohort Study. Clin. Infect. Dis. 48, 1459–1466.

Khemici, V., Poljak, L., Luisi, B.F., Carpousis, A.J., 2008. The RNase E of *Escherichia coli* is a membrane-binding protein. Mol. Microbiol. 70 (4), 799–813.

Knowles, W.A., Pipkin, P., Andrews, N., Vyse, A., Minor, P., Brown, D.W., Miller, E., 2003. Population-based study of antibody to the human polyomaviruses BKV and JCV and the simian polyomavirus SV40. J. Med. Virol. 71 (1), 115–123.

Kumar, Y., Cocchiaro, J., Valdivia, R.H., 2006. The obligate intracellular pathogen Chlamydia trachomatis targets host lipid droplets. Curr. Biol. 16 (16), 1646–1651.

Leuenberger, D., Andresen, P.A., Gosert, R., Binggeli, S., Strom, E.H., Bodaghi, S., Rinaldo, C.H., Hirsch, H.H., 2007. Human polyomavirus type 1 (BK virus) agnoprotein is abundantly expressed but immunologically ignored. Clin. Vaccine Immunol. 14 (8), 959–968.

Linstedt, A.D., Hauri, H.P., 1993. Giantin, a novel conserved Golgi membrane protein containing a cytoplasmic domain of at least 350 kDa. Mol. Biol. Cell 4 (7), 679–693.

Liu, P., Bartz, R., Zehmer, J.K., Ying, Y.S., Zhu, M., Serrero, G., Anderson, R.G., 2007. Rab-regulated interaction of early endosomes with lipid droplets. Biochim. Biophys. Acta 1773 (6), 784–793.

Miyanari, Y., Atsuzawa, K., Usuda, N., Watashi, K., Hishiki, T., Zayas, M., Bartenschlager, R., Wakita, T., Hijikata, M., Shimotohno, K., 2007. The lipid droplet is an important organelle for hepatitis C virus production. Nat. Cell Biol. 9 (9), 1089–1097.

Moriyama, T., Sorokin, A., 2008. Repression of BK virus infection of human renal proximal tubular epithelial cells by pravastatin. Transplantation 85 (9), 1311–1317.

Myhre, M.R., Olsen, G.H., Gosert, R., Hirsch, H.H., Rinaldo, C.H., 2010. Clinical polyomavirus BK variants with agnogene deletion are non-functional but rescued by trans-complementation. Virology (Electronic publication ahead of print).

Nast, C.C., Cohen, A.H., 1985. Renal cholesterol granulomas: identification and morphological pattern of development. Histopathology 9 (11), 1195–1204.

Ostermeyer, A.G., Ramcharan, L.T., Zeng, Y., Lublin, D.M., Brown, D.A., 2004. Role of the hydrophobic domain in targeting caveolin-1 to lipid droplets. J. Cell Biol. 164 (1), 69–78.

Padgett, B.L., Walker, D.L., ZuRhein, G.M., Eckroade, R.J., Dessel, B.H., 1971. Cultivation of papova-like virus from human brain with progressive multifocal leucoencephalopathy. Lancet 1 (7712), 1257–1260.

Ramos, E., Drachenberg, C.B., Wali, R., Hirsch, H.H., 2009. The decade of polyomavirus BK-associated nephropathy: state of affairs. Transplantation 87 (5), 621–630.

Rinaldo, C.H., Hirsch, H.H., 2007. Antivirals for the treatment of polyomavirus BK replication. Expert Rev. Anti. Infect. Ther. 5 (1), 105–115.

Rinaldo, C.H., Traavik, T., Hey, A., 1998. The agnogene of the human polyomavirus BK is expressed. J. Virol. 72 (7), 6233–6236.

Rust, R.C., Landmann, L., Gosert, R., Tang, B.L., Hong, W., Hauri, H.P., Egger, D., Bienz, K., 2001. Cellular COPII proteins are involved in production of the vesicles that form the poliovirus replication complex. J. Virol. 75 (20), 9808–9818.

Safak, M., Barrucco, R., Darbinyan, A., Okada, Y., Nagashima, K., Khalili, K., 2001. Interaction of JC virus agno protein with T antigen modulates transcription and replication of the viral genome in glial cells. J. Virol. 75 (3), 1476–1486.

Schweizer, A., Fransen, J.A., Bachi, T., Ginsel, L., Hauri, H.P., 1988. Identification, by a monoclonal antibody, of a 53-kD protein associated with a tubulo-vesicular compartment at the cis-side of the Golgi apparatus. J. Cell Biol. 107 (5), 1643–1653.

Schweizer, A., Ericsson, M., Bachi, T., Griffiths, G., Hauri, H.P., 1993. Characterization of a novel 63 kDa membrane protein. Implications for the organization of the ER-to-Golgi pathway. J. Cell Sci. 104, 671–683.

Shishido-Hara, Y., Ichinose, S., Higuchi, K., Hara, Y., Yasui, K., 2004. Major and minor capsid proteins of human polyomavirus JC cooperatively accumulate to nuclear domain 10 for assembly into virions. J. Virol. 78 (18), 9890–9903.

Subramanian, V., Garcia, A., Sekowski, A., Brasaemle, D.L., 2004. Hydrophobic sequences target and anchor perilipin A to lipid droplets. J. Lipid Res. 45 (11), 1983–1991.

Suzuki, T., Okada, Y., Semba, S., Orba, Y., Yamanouchi, S., Endo, S., Tanaka, S., Fujita, T., Kuroda, S., Nagashima, K., Sawa, H., 2005. Identification of FEZ1 as a protein that interacts with JC virus agnoprotein and microtubules: role of agnoprotein-induced dissociation of FEZ1 from microtubules in viral propagation. J. Biol. Chem. 280 (26), 24948–24956.

Urahama, Y., Ohsaki, Y., Fujita, Y., Maruyama, S., Yuzawa, Y., Matsuo, S., Fujimoto, T., 2008. Lipid droplet-associated proteins protect renal tubular cells from fatty acid-induced apoptosis. Am. J. Pathol. 173 (5), 1286–1294.

van Kuppeveld, F.J., Hoenderop, J.G., Smeets, R.L., Willems, P.H., Dijkman, H.B., Galama, J.M., Melchers, W.J., 1997. Coxsackievirus protein 2B modifies endoplasmic reticulum membrane and plasma membrane permeability and facilitates virus release. EMBO J. 16 (12), 3519–3532.

Welte, M.A., 2007. Proteins under new management: lipid droplets deliver. Trends Cell Biol. 17 (8), 363–369.

White, M.K., Khalili, K., 2005. Expression of JC virus regulatory proteins in human cancer: potential mechanisms for tumourigenesis. Eur. J. Cancer 41 (16), 2537–2548.

Zehmer, J.K., Huang, Y., Peng, G., Pu, J., Anderson, R.G., Liu, P., 2009. A role for lipid droplets in inter-membrane lipid traffic. Proteomics 9 (4), 914–921.